



Sub-micron structuring/texturing of diamond-like carbon-coated replication masters with a femtosecond laser

Aleksandra Michalek¹ · Shaojun Qi² · Afif Batal¹ · Pavel Penchev¹ · Hanshan Dong² · Tian Long See³ · Stefan Dimov¹

Received: 4 November 2019 / Accepted: 9 January 2020 / Published online: 1 February 2020
© The Author(s) 2020

Abstract

Diamond-like carbon (DLC) coatings have very attractive mechanical and tribological properties, i.e. high hardness, low friction and high wear resistance. Therefore, DLC is often used as a solid lubricant in moulds for injection moulding. Laser processing of DLC with ultrashort lasers, i.e. femtosecond lasers, can be performed both at micron and sub-micron scales, namely by producing laser-induced periodic surface structures (LIPSS). In this research, the effects of laser structuring/texturing on DLC properties are investigated. First, the laser-processing parameters were optimised to produce uniform LIPSS without damaging a thin DLC film and then the properties of the textured DLC-coated substrates were studied. It was determined that the tribological properties of the processed surfaces remained unchanged, but the hardness of the structured/textured DLC layers was reduced significantly. Although GAXRD and Raman spectroscopy did not show any significant crystallisation of the DLC coating after the laser irradiation, the analysis indicated that a thin graphitised layer had been formed on the surface as a result of the femtosecond laser processing.

Keywords LIPSS · Diamond-like carbon (DLC) · Femtosecond laser · Laser microprocessing

1 Introduction

Diamond-like carbon (DLC) coating is an amorphous form of carbon with a significant fraction of tetrahedral (sp^3) bonds [1]. The coating stands out among others for its high hardness, low friction coefficient, low adhesion, small surface roughness, optical transparency [2] and chemical inertness. Some of its properties are similar to those of diamond because of the presence of diamond-like bonds and also mostly because the isotropic disordered thin film does not possess any grain boundaries [3]. At the same time, they are cheaper to produce and therefore DLC coatings are widely used in various applications, i.e. as protective and wear-resistant coatings in biomedical implants [4],

microelectronic devices [5], as infrared optical windows and in magnetic storage discs [6].

DLC coatings also can be applied as solid lubricant to increase the durability and reduce the demoulding forces in injection moulding. The effectiveness of DLC coatings in this process was studied and it was found that the replication performance together with the component's life span was improved [7]. In particular, it was possible to produce a higher number of replicas with acceptable quality, while the tool wear was minimised, i.e. the sharp edges on the mould were preserved during a higher number of cycles without the need to clean or replace the mould. Another benefit associated with the use of DLC coatings in the microinjection moulding process is its lower thermal expansion compared with common steel moulds. This could increase the tool life by preventing delamination, cracking and coating failures. However, a good adhesion between the DLC coating and the mould is necessary and a proper selection of the tooling material, thermoplastics and moulding process parameters is required [8]. Additionally, due to DLC's lubricating properties and low surface roughness, the ejection forces in microinjection moulding of components with large area to volume ratios surfaces can be decreased significantly [9]. Also, the

✉ Aleksandra Michalek
AMM752@bham.ac.uk

¹ School of Mechanical Engineering, University of Birmingham, Edgbaston, Birmingham B15 2TT, UK

² School of Metallurgy and Materials, University of Birmingham, Edgbaston, Birmingham B15 2TT, UK

³ The Manufacturing Technology Centre Ltd, Pilot Way, Ansty Park, Coventry CV7 9JU, UK

same effect was observed on DLC-coated mould tools with sub-micron textures (nano bead-like features and nanopillars fabricated by photolithography) and this was explained with the low coefficient of friction (CoF) as a dominant factor in achieving low demoulding forces [10]. It is worth noting that these investigations were conducted using relatively thick DLC coatings up to 5 μm , which were applied on completely machined moulds and thus their properties remained intact. However, if sub-micron structuring of the moulds is required, this should be performed only after DLC is applied and it should be stressed that any processing, including laser, should not alter the coating's properties. In this way, DLC's advantageous properties could be combined with those of micro- and nano-patterned/textured surfaces. So far, improving DLC's properties was achieved by either strengthening DLC with titanium or nitrogen doping [7] or by microscale patterning of the coating with a nanosecond laser, resulting in 30% CoF improvements [11]. Also, it was reported that the friction properties could be preserved or even improved after femtosecond (fs) laser sub-micron structuring, although this was dependent on the contact material and laser pulse energy [12, 13]. CoF as low as 0.02 was achieved when an additional layer of MoS₂ was applied on top of the laser-structured DLC [14].

Laser-induced periodic surface structures (LIPSS) are known for their optical [15], antibacterial, biological [16] and hydrophobic properties among their other surface functionalisation applications. Such surface responses had been achieved by optimising the process and thus to produce structures with specific geometric characteristics, e.g. to generate uniform and homogenous LIPSS by obtaining and maintaining the most effective light diffraction. LIPSS are formed on surfaces at process settings near the ablation threshold of a given material due to interference of incident laser light with excited surface electromagnetic wave [17]. Their sub-micron periodicity depends on the laser source wavelength and dielectric constants of the material, while their orientation is normal to the beam polarisation vector and their amplitudes can be varied by controlling the laser fluence level [18].

Synergistic effects can be sought by fabricating LIPSS on replication masters with DLC films, especially to improve both their wear resistance, i.e. the tool durability with regard to the surfaces' functional response, and also the quality of replicas because of DLC lubricating properties. However, laser irradiation of amorphous materials, such as DLC, can lead to structural changes and thus alter their properties. Laser processing of DLC was already reported and pulse duration was identified as the most important factor governing the resulting coating's structure. Longer pulses and higher intensity led to graphitisation, spallation and evaporation and thus creating swelling, delamination and removal of the DLC layer at the end. In addition, surface morphology

changes have been observed that are common in carbon-based materials, for instance a structural transformation into glassy carbon (GC) [19]. This carbon material has sp³ content close to 0% and benefits from higher conductivity, thermal resistance and similar frictional properties to DLC, but its wear resistance is inferior [20]. Therefore, it was concluded that longer pulses, pico- and nanosecond, and higher ranges were not suitable for patterning/structuring of DLC films. At the same time, femtosecond laser processing has emerged as a promising technology for a very controllable generation of fine and precise structures, both at micron and sub-micron scale with minimised thermal effects.

In this research, the effects of the femtosecond laser-processing parameters in producing homogenous and uniform LIPSS on DLC coating were investigated with a special focus on their resulting properties. Especially, an LIPSS treatment of steel substrates with DLC films was studied as a one-step approach for producing functional and, at the same time, durable surface structures/textures for replication masters.

2 Materials and methods

A thin DLC film was deposited on 2.5 mm-thick 316L stainless steel substrates by employing a plasma-assisted chemical vapour deposition (PACVD) to produce a coating with 2–5 μm thickness, 22 GPa hardness (equivalent of HV 2500) and 0.05 μm surface roughness. The DLC film was irradiated with a femtosecond ytterbium-doped fibre laser source with the following technical characteristics: a near infrared wavelength (λ) of 1030 nm, pulse duration of 310 fs and maximum pulse energy of 10 μJ . A linearly polarised laser beam was focused with 100 mm telecentric lens on the substrate surface to achieve a beam spot diameter (d_b) of 40 μm at $1/e^2$ of Gaussian profile intensity. A schematic scanning strategy of an area is illustrated in Fig. 1. In particular, the area was irradiated with trains of laser pulses with a fixed hatch distance (h) between them of 3 μm that resulted in 92.5% pulse overlap in the Y direction, while the pulse distance in the X direction was varied with scanning speed (v) and frequency (f) and thus to control the LIPSS uniformity. The pulse fluence was calculated as follows:

$$F = \frac{4P}{f\pi d_b^2} \quad (1)$$

where P is the average power (W).

The effects of accumulated fluence (F_{acc}) on the resulting LIPSS were investigated in this research by varying the number of pulses per spot (pps) when structuring an area. pps were calculated as follows:

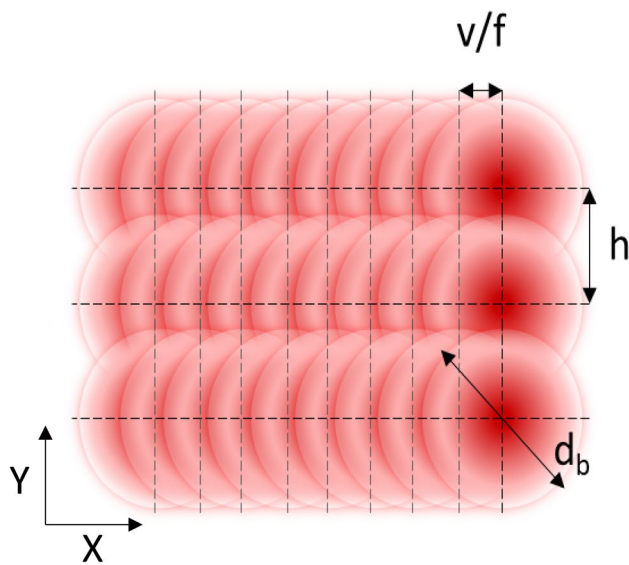


Fig. 1 A schematic illustration of an area processed with multiple pulse trains with pulses overlapping in X direction governed by scanning speed (v) and frequency (f) and in Y direction, overlapping is dependent on hatch offset (h) between the pulse trains

$$\text{pps} = \frac{f \cdot d_b}{v} \quad (2)$$

However, Eq. 2 defines only pps along one pulse train. However, for structuring an area multiple pulse trains/scan lines are required with h offset between them. Hence, there is a pulse overlap in the Y direction, too, especially when $h < d_b$, and then the total number of pulses per spot ($\text{pps}_{\text{total}}$) can be calculated as follows:

$$\text{pps}_{\text{total}} = \frac{f \cdot d_b}{v} + \frac{d_b}{h} \quad (3)$$

Thus, when multiple trains of pulses are required to process an area, $\text{pps}_{\text{total}}$ should be taken into account in calculating F_{acc} .

The topographies of the processed surfaces were analysed with atomic force microscope (AFM) and scanning electron microscope (SEM) to study the LIPSS geometrical characteristics and at the same time to detect any damage to the DLC coating. The LIPSS periodicity was determined by performing 2D fast Fourier transformation (2D FFT) of the images while their uniformity was assessed visually, where no non-processed areas or highly irregular ripples were observed.

CoF and wear resistance of textured DLC films were measured with a ball-on-plate tribometer at room temperature under dry condition. Linear reciprocating tests were performed using an alumina ball of 8 mm diameter with a hardness of approximately 16 GPa (HV 1600). The distance of the lines was 4 mm per cycle and the reciprocating

movements were executed with a speed of 2 mm/s. The load applied on the DLC film was 150 g (1.47 N).

Raman spectra were recorded from 100 to 3200 cm^{-1} using a 633 nm laser source with a focused spot size of approximately 2 μm . Axial and lateral resolutions were less than 1 μm and 0.25 μm , respectively. The resulting spectra were fitted with Lorentzian and Breit–Wigner–Fano (BWF) profiles for D and G peaks, respectively, with a linear baseline correction for the background. The peak position and the full width at half-maximum (FWHM) were calculated.

The DLC crystalline structure was analysed with glancing angle X-ray diffraction (GAXRD) with a cobalt source at an incident angle of 3°. The penetration of the X-ray beam was within the DLC film thickness and thus to detect easily any long-range crystallisation into the laser-processed DLC.

The hardness of as-received and laser-processed DLC films were measured by conducting a nanoindentation test. An indenter with a tip radius of 50 nm was used ten times on each sample by applying a load with a depth control of 400 nm. In this way, any periodic sub-micron structures present on the surface were less likely to affect the hardness measurements and also the indentation depth was within the recommended less than 10% thickness of the coating.

3 Results and discussion

3.1 LIPSS optimisation

3.1.1 Single spot irradiation

Two types of LIPSS can be distinguished when their periodicity (Λ) is considered, i.e. low spatial frequency LIPSS (LSFL) and high spatial frequency LIPSS (HSFL). LSFL has a Λ close to the laser source wavelength (λ), while the ripples are perpendicular to the beam polarisation vector. On the other hand, HSFL has a Λ much smaller than λ and their orientation can be either parallel or perpendicular to the beam polarisation vector [21].

Single spots were irradiated onto DLC with varied processing settings, i.e. the number of pulses and fluence, to study the LIPSS generation from their development onto the surface.

Five representative SEM images of LIPSS evolution as a result of the increasing pulse and accumulated fluence are provided in Fig. 2. One pulse irradiation did not result in any surface damage and only after 20 pulses (see Fig. 2a) HSFL gradually appeared around the spot periphery with periodicity of approximately 140 nm ($\sim 0.1\lambda$). At the same time, LSFL generation was observed at the spot centre where the intensity was much higher. A further increase of the number of pulses to 50 led to the generation of straight and uniform LSFL as depicted in Fig. 2c, while there was a fraction of

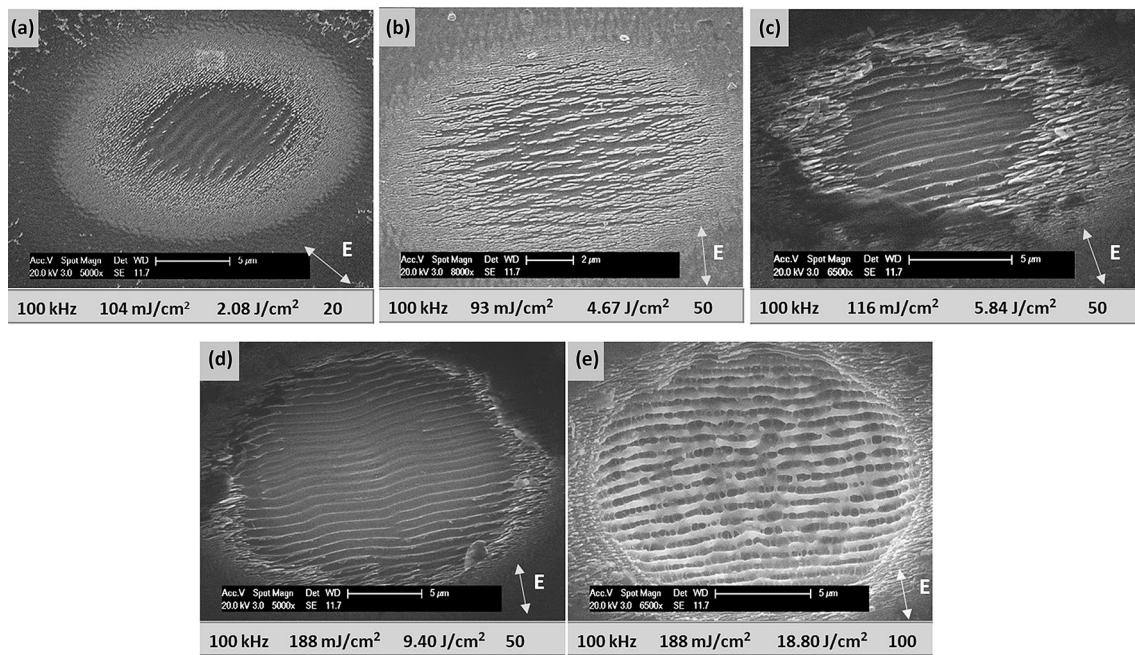


Fig. 2 Single spots irradiated with a fs laser source and varying pulse numbers and fluence. Note: (1) the processing parameters, i.e. frequency, pulse fluence, accumulated fluence and number of pulses,

used for the LIPSS generation are provided below the corresponding SEM images; (2) the double arrow indicates the polarization direction

HSFL around the spot edge. Such observation is caused by the Gaussian distribution of the laser beam where the laser energy decreases at the peripheral of the beam spot. As can be seen in Fig. 2d, further increase of pulse fluence but same number of pulses led to bigger area of uniform LSFL and reduced fraction of HSFL. Hence, the threshold fluence for HSFL generation is lower than that for LSFL [22]. On the contrary, the same number of pulses but with a lower fluence resulted in the formation of LSFL and HSFL across the spot area (Fig. 2b). Ablation of the DLC film at the spot centre can be observed at pps of 100, but also LSFL and HSFL are visible around the spot edge together with some molten material (see Fig. 2e). Thus, the LIPSS evolution from HSFL to LSFL and the removal of the DLC film with the increase of pulse number clearly show that an optimal accumulated fluence, both pulse fluence and number of pulses above the respective thresholds, is required for achieving a homogenous LIPSS generation. In this research, the focus is on homogenous LSFL generation onto the DLC films (later referred as LIPSS only) as they are commonly investigated when LIPSS are employed to the functional response of surfaces.

3.1.2 Large area structuring

An LIPSS treatment of replication masters with DLC films is the focus of this research and therefore the process settings should be optimised for large area structuring. Thus,

a processing window to achieve uniform LIPSS coverage of large areas without damaging the DLC coating and any excessive ablation are identified. The parameter domain investigated has a fluence and pps of 58–130 mJ/cm² and 14 to 33, respectively, as shown in Fig. 3a. The scan lines' offset, h , was kept constant and thus pps_{total} resulted in a range from 28 to 47. The uniformity of the resulting LIPSS was assessed and any visible DLC damage was identified, especially when the stainless steel substrate underneath was revealed. It is worth noting that the use of process parameters outside the investigated parameter domain led to an ablation of the coating or the generation of non-uniform LIPSS over the processing area. The increase of fluence and pps_{total} improves LIPSS uniformity. Therefore, the processing window investigated in this research (see Fig. 3a) was defined by taking both, uniformity of LIPSS and damage of DLC, into consideration. The DLC characterisation work was performed on three representative samples, i.e. S1, S2 and S3, chosen at the window boundaries or just outside the tested parameters and one, S4, at its centre. The surface topographies of the four samples are depicted in Fig. 3b with their respective laser-processing parameters underneath the images. It should be noted that fluence used for sample S3 of 66 mJ/cm² was selected to be close to the processing window, but not too similar to the laser intensity employed on the other three samples.

Considering the results from the single pulse irradiation (see Sect. 3.1.1), it can be stated that LIPSS produced

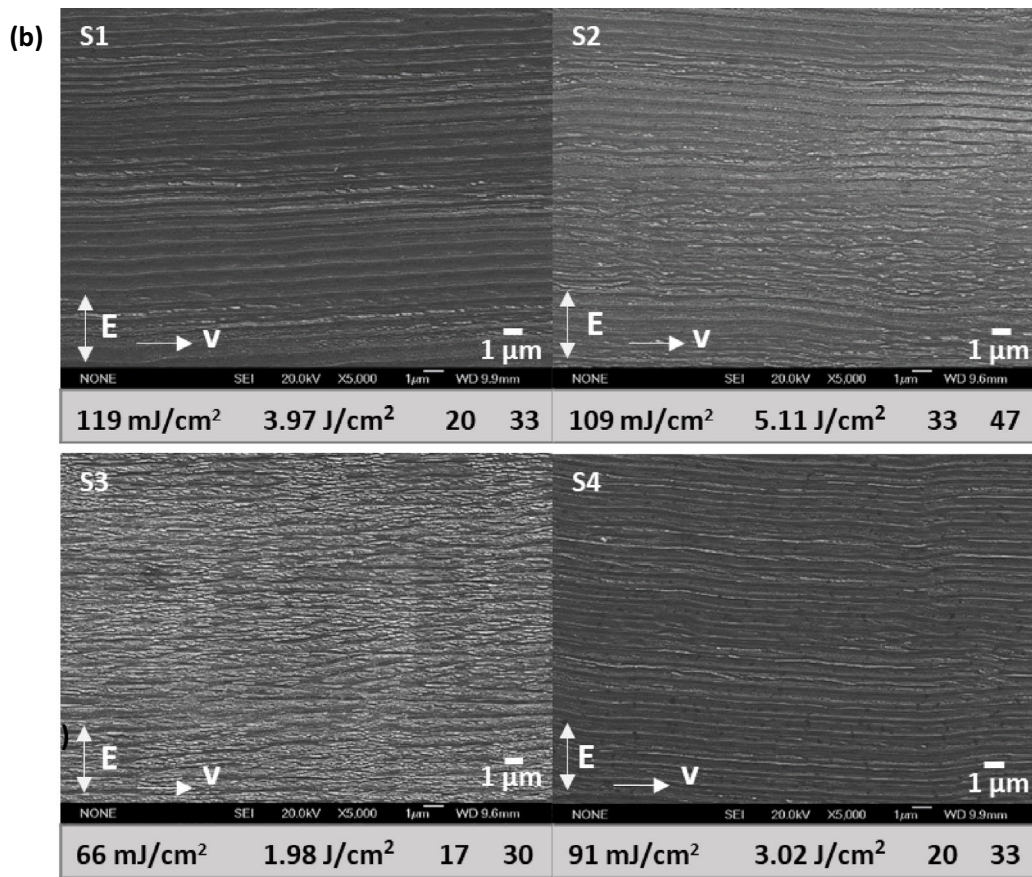
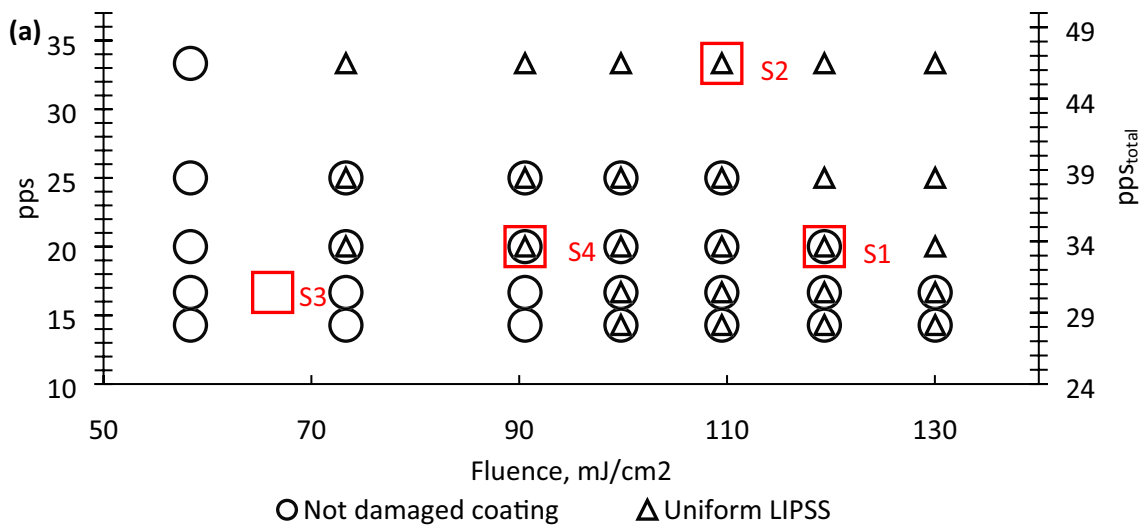


Fig. 3 The results obtained with large area structuring: **a** the effects of pulses per spot (pps) and fluence levels on LIPSS uniformity across the studied processing domain; **b**) SEM images of S1, S2, S3 and S4 samples (red squares in **a**)). Note: (1) the processing param-

eters: F , F_{acc} , pps and pps_{total} , are provided below the corresponding SEM images; (2) the double arrow (E) indicates the polarization direction while the single arrow the scanning direction (v)

with a multiple pulse trains over large areas are of similar characteristics where F_{acc} used is marginally lower than that applied for LIPSS generation with a single spot irradiation. A close look at the LIPSS morphologies in

Fig. 3b suggests that HSFL are still present, but they are more pronounced on S3. The used pps_{total} and F for this sample were the lowest and thus also F_{acc} was the lowest, resulting in ripples similar to those depicted in Fig. 2 I

where LSFL were wavy and irregular. At the same time, the LIPSS straightness on S1 and S4 is better, while HSFL are less visible due to higher F despite similar pps_{total} . S2 was produced with the highest process settings, i.e. F and pps_{total} , and thus F_{acc} was the highest, too. Therefore, LIPSS were well defined but at the same time there were some areas on the surface where the DLC film was much thinner and with some initial signs of delamination were present (not shown in Fig. 3b).

It was observed that the LIPSS periodicity achieved with the optimised process setting was in the range of 700–800 nm ($\sim 0.7\text{--}0.8\lambda$). This was lower than the commonly observed LIPSS periodicity range from 800 to 950 nm on steel substrates with the same laser wavelength and could be partially attributed to the differences between steel and DLC optical constants, in particular refractive index and extinction coefficient. The height of the produced ripples was 200 nm on average and was consistently obtained across the studied processing domain.

3.2 Characterisation

3.2.1 Raman spectroscopy

Laser-treated and as-received DLC samples were analysed employing Raman spectroscopy that is considered a reliable way to obtain structural information and also to judge about the quality of carbon materials. The DLC-specific spectrum shown in Fig. 4 consists of two sp^2 -carbon characteristic modes: D ('disorder'—'ring' type bond) and G ('graphite'—both 'ring' and 'chain' types) with positions of 1268 cm^{-1} and 1509 cm^{-1} , respectively. The ratio between D and G peak, i.e. $I(D)/I(G)$, can be used as an indication of the fraction of graphite-like (sp^2 aromatic rings) domains in a DLC thin film. Fitting results are provided in Table 1. The D and G peak positions differ from the ones reported usually as 1355 cm^{-1} and 1550 cm^{-1} due to a higher Raman laser wavelength used in this study, which causes the peaks shift towards lower wavenumbers [3]. The spectrum is dominated by the sp^2 sites up to 230 times more when compared to sp^3 due to higher polarisability of π states, typical for this

Fig. 4 Raman spectra of as-received DLC and its deconvolution: linear background together with Lorentzian and Breit–Wigner–Fano fitting lines for D and G peaks, respectively

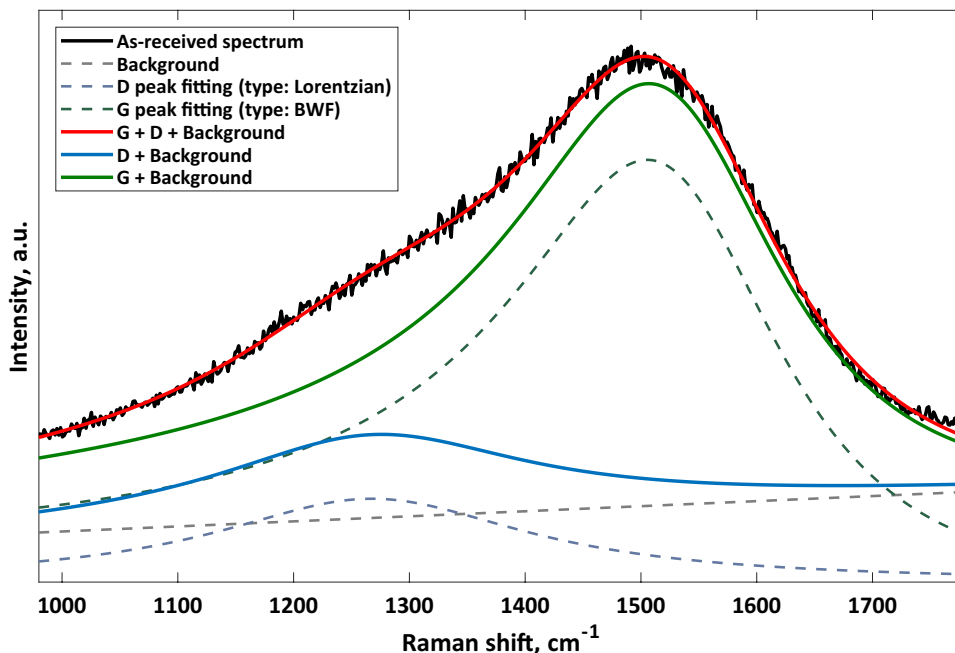


Table 1 Results of G and D peaks' fitting for as-received and laser-textured DLC samples

Sample	G position, cm^{-1}	G FWHM, cm^{-1}	D position, cm^{-1}	D FWHM, cm^{-1}	$I(D)/I(G)$	Fitting error, %
S1	1590 ± 3	136 ± 42	1340 ± 6	294 ± 37	1.06	3.35
S2	1591 ± 5	132 ± 45	1338 ± 5	294 ± 46	1.12	2.95
S3	1587 ± 11	135 ± 136	1335 ± 7	293 ± 89	1.23	2.91
S4	1590 ± 6	133 ± 38	1335 ± 6	298 ± 67	1.16	2.30
As received	1509 ± 3	286 ± 8	1268 ± 11	330 ± 49	0.20	1.26

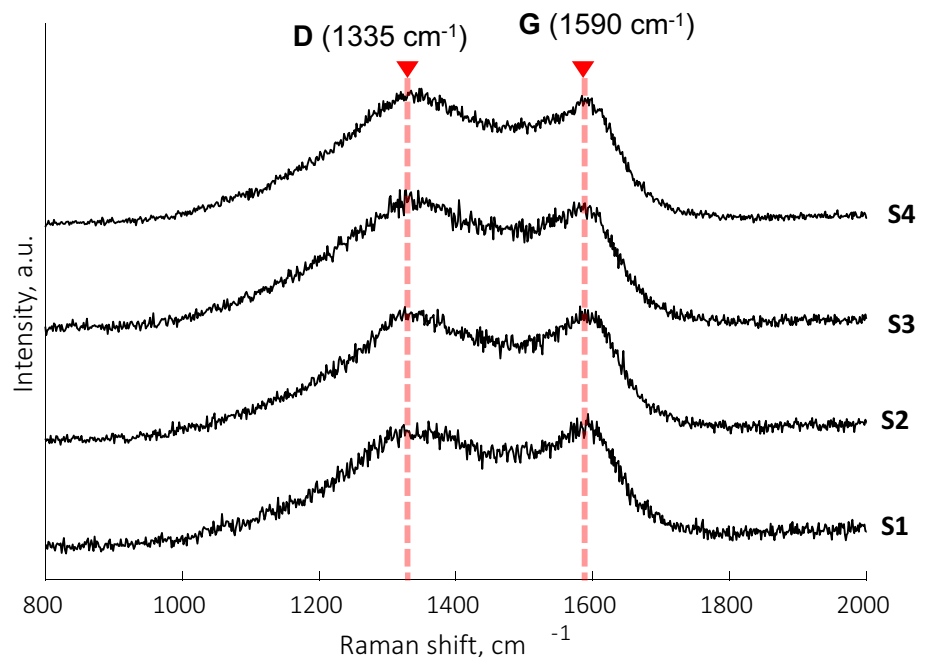
type of bonding [3]. The position of G peak is at 1570 cm^{-1} and intensity $I(D)/I(G)$ ratio is close to 0 (for Raman data at 514 nm) in case of ideal ta-C DLC coatings with high fraction of sp^3 bonds (above 70%) [1]. It was reported for laser patterned DLC with ns laser pulses that the G position shifted to higher wavenumbers, while D intensity increased with the increase of fluence, and this indicated a progressive laser-induced graphitisation of the amorphous DLC [23, 24]. After the femtosecond laser treatment of four samples, the spectra of which are shown in Fig. 5, it is visible that the G peak shifted to 1590 cm^{-1} . The intensity ratio of two peaks $I(D)/I(G)$ increased from 0.2 on the as-received DLC to above 1.0 for the laser-patterned surface. Even though these changes in spectra could indicate an induced graphitisation of the thin film, there are no substantial changes between the four laser-structured samples that have been produced with different laser processing parameters. This might be because the ultrashort pulsed laser processing did not introduce any heating into the material and/or the differences in laser-processing parameters between the samples were minor. Raman spectra were also obtained on the samples produced with a lower number of pps and higher fluence, and still there were no further shifts in the peaks or intensities. The similar spectra suggest that the increase of fluence did not initiate further changes in the DLC short ordering.

The interaction between ultrashort pulses and carbon phases should be properly explained to further understand the resulting change in Raman spectra. Studies reported that fs laser pulses induced non-equilibrium transition of

sp^3 to sp^2 bonds [25]. Additionally, simulations revealed that a layer-by-layer graphitisation could occur within the optical depth of diamond absorption [26], whereas for longer pulses graphitisation would propagate into the bulk due to heat dissipation and thus temperatures above the graphitisation threshold could be reached [19]. The thickness of such graphitised layers would be dependent on pulse numbers and fluence with a depth limitation of hundreds of nanometres (up to 200 nm). In addition, it was reported that the resulting Raman spectra of DLC processed with ns and fs pulses did not differ significantly, though it was stated that their graphitised layers led to structural distinctions [27]. Other researchers suggested that fs laser-processed DLC would be modified into glassy carbon (GC), a form of carbon with 100% sp^2 and sp^3 content close to 0% with a hardness of 3 GPa [3], but with similar D and G peak position [28]. A further increase of processing fluence would lead to Raman results similar to the spectra of superimposed GC, DLC and carbonaceous materials [29]. However, the penetration depth of Raman laser sources can be higher than modified layers and thus the laser can excite not only the modified layers, but also non-modified DLC.

Overall, it can be stated that fs laser processing did not trigger significant changes in the bulk DLC structure and only a thin laser-modified surface layer was graphitised. However, the LIPSS amplitude is of similar scale and therefore this fact cannot be neglected. Additionally, mechanical properties of such graphitised layers are quite different and inferior when compared to as-received DLC.

Fig. 5 Raman spectra of four fs laser processed DLC samples



3.2.2 Glancing angle X-ray diffraction

A further analysis was conducted with GAXRD to investigate the resulting structural changes in the laser-treated DLC. The results obtained on as-received and laser-modified DLC are shown in Fig. 6. Samples S2 and S3 were chosen for this additional analysis, as the laser settings used in their processing were the most distinct (see Fig. 3). It was confirmed that the first and third peaks visible in Fig. 6 come from the austenite in the substrate, i.e. the steel plates that were coated with DLC. The second small peak could be attributed to either ferrite within the austenitic stainless steel or chromium coming from the buffer layer between the DLC and steel substrate as they have similar crystal structures. The difference in intensities or the small shifts could be explained with some misalignment on the surface level during the measurements that were more pronounced in GAXRD. No graphite crystallisation was detected by this GAXRD measurement implying the absence of DLC crystallisation or crystallite size changes after laser processing were too small to detect by X-ray. In addition, if the laser modified layer thickness is less than 200 nm (see Sect. 3.2.1), any signal coming from such a thin layer could be too weak to detect. If any substantial graphite crystallisation at micro- or nanoscale was present, a broad peak would have appeared at approximately 26° or 50° [30].

3.2.3 Nanoindentation

It is not easy to assess the actual hardness of LIPSS onto the DLC films due to the ripples influence on the surface and also the relatively soft substrate material. The results from the nanoindentation measurements are summarised in Fig. 7

where a distinct hardness reduction of DLC coating can be seen after the fs laser processing. The hardness has been reduced from 22 GPa to approximately 9 GPa for sample S3, even though low fluence and less pps have been used. These changes could be attributed mostly to the modifications in the DLC thin layer after the fs laser processing and to a lesser extent to the presence of LIPSS (see Sect. 3.2.1). Another evidence for this effect is that the further increase of fluence and pps led to even bigger hardness reduction of approximately 4 GPa on sample S2. For comparison, the hardness of the substrate is normally around 2.5 GPa. All these suggest that the DLC film is sensitive to the used laser-processing parameters and even small changes can lead to substantial deviations of resulting nanohardness. The other reason for the distinct hardness reduction could be the wavy profile of LIPSS on the surface that could affect the indentation contact and thus the obtained hardness values.

3.2.4 Ball-on-plate tests

The results from the CoF measurements on fs laser-processed and as-received DLC after 100 ball-on-plate cycles are provided in Fig. 8. It can be seen that up to 50 cycles, there were no visible changes in the friction properties between as-received and laser-processed samples. However, a slight CoF increase on processed samples was observed after 50 cycles. This can be explained by the increased contact area between the ball and the LIPSS-treated plates as depicted in Fig. 9. All four fs laser-treated samples did not demonstrate significant CoF differences with the increase of the ball-on-plate cycles, in spite of the exhibited changes in their mechanical properties, e.g. their hardness. Taking into account the presence of the thin modified layer discussed in

Fig. 6 GAXRD spectra of DLC coatings on as-received and S2 and S3 samples after fs laser processing

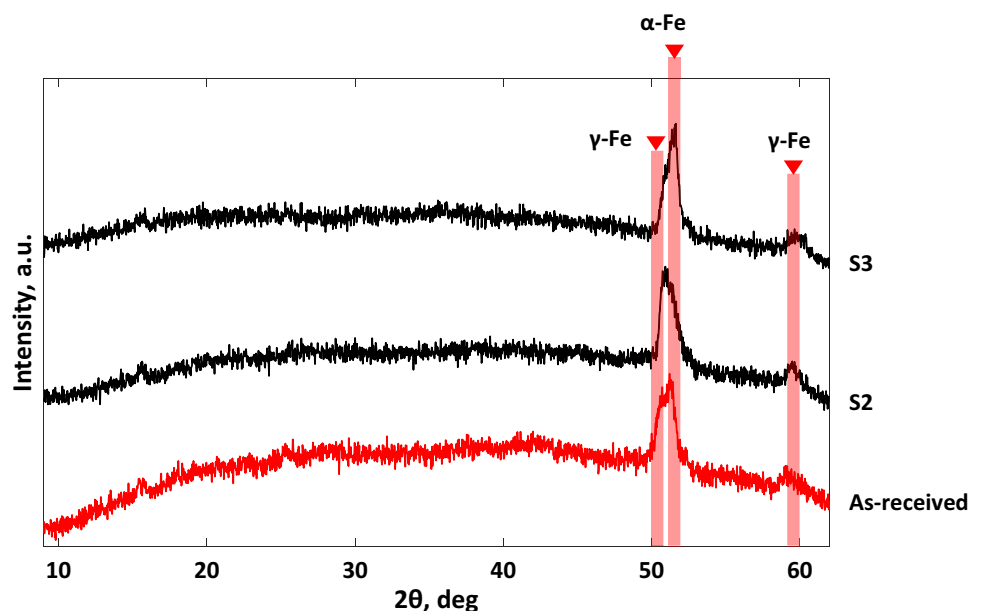


Fig. 7 Nanoindentation results of as-received and laser textured DLC

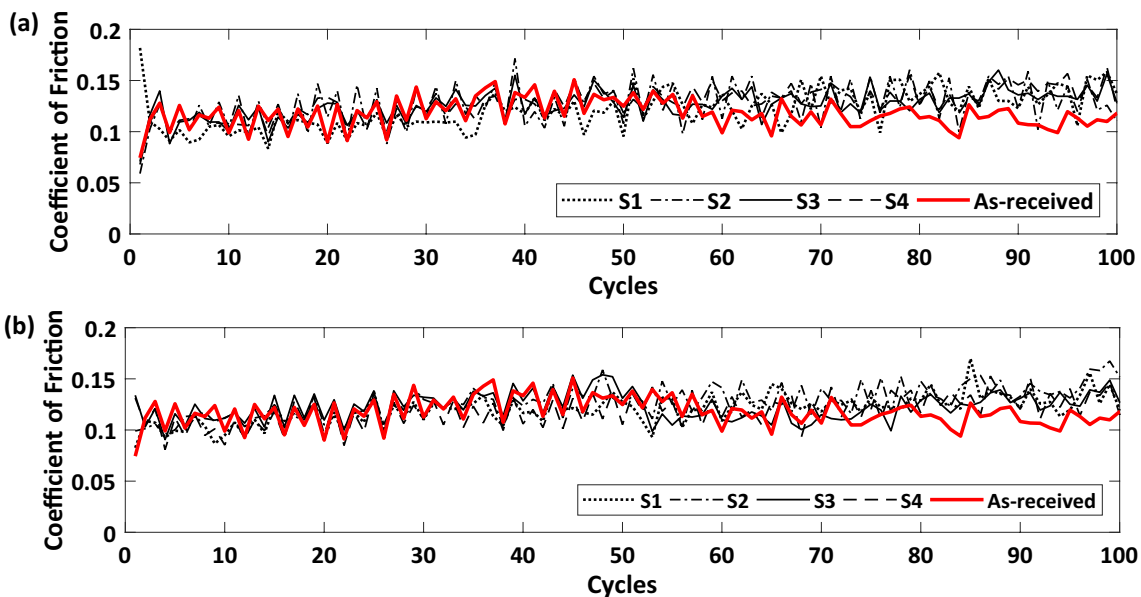
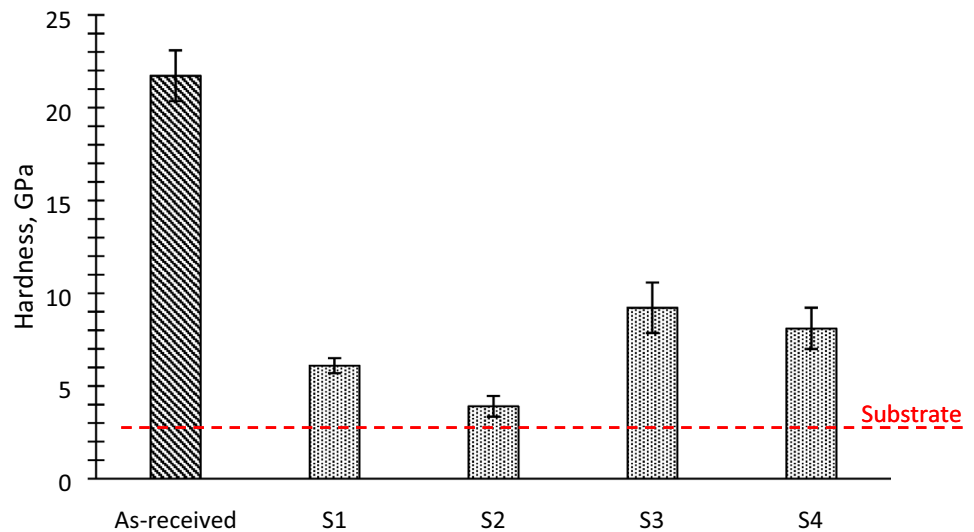


Fig. 8 Measured CoF for 100 cycles for as received and laser patterned DLC samples with reciprocating direction perpendicular (a) and parallel (b) to LIPSS

Sect. 3.2.1 that is structurally similar to GC, these results are expected because of the comparable tribological performance of both materials. In particular, it was reported that GC had CoF of around 0.2 when alumina balls were used in the tests [31], while a mean CoF value of 0.12 was obtained in this research on as-received DLC. Interestingly, the same CoF trends were observed during reciprocating tests performed perpendicular and parallel to LIPSS, as can be seen in Fig. 8a,b. In addition, the wear tracks had similar widths, too, and thus the orientation of periodic structures did not influence the CoF measurements, but mostly the contact of the laser-modified DLC with the ball.

After examining the wear track with the focus variation microscope, the track did not have any noticeable depth at macroscale or the material removal was too small to detect. Additional AFM measurements were conducted that revealed smudged LIPSS and the surface looked like having been polished as depicted in Figs. 9 and 10. Further EDS inspections did not detect any alumina traces in the wear track and thus to suggest that any debris came from the modified DLC. Apparently, the graphitised layer filled the valleys of the ripples during the ball reciprocating movements and as a result the LIPSS profiles became shallower (Fig. 10). This cannot be considered unexpected, as at this

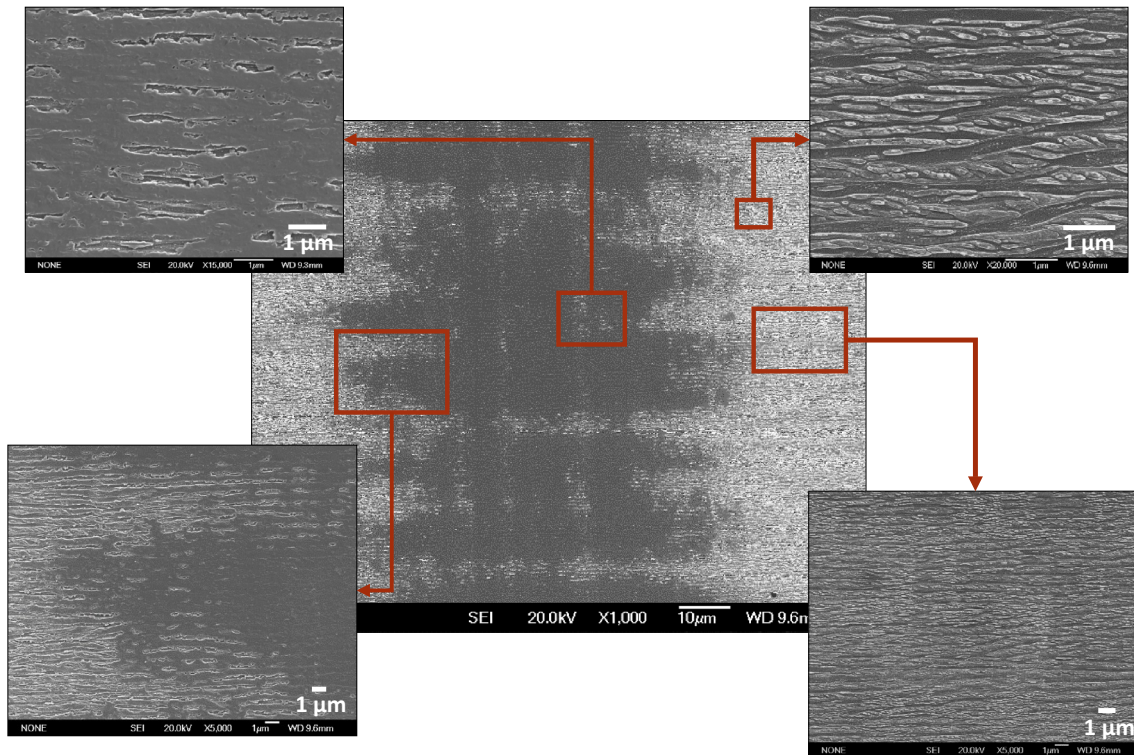
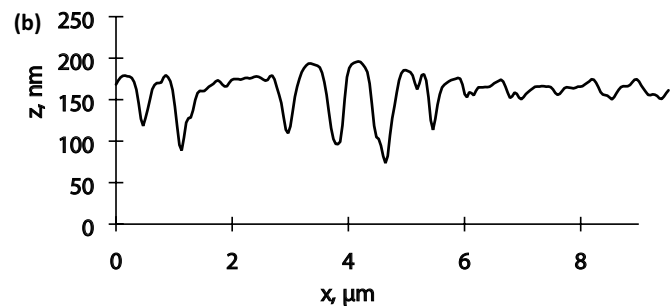
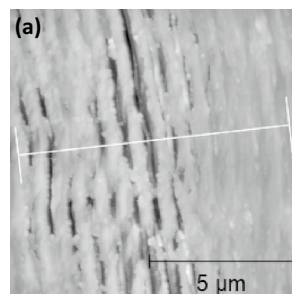


Fig. 9 SEM images of wear tracks of sample S3 after 50 reciprocating cycles perpendicular to LIPSS

Fig. 10 AFM measurements: **a** a sample S3 after 100 reciprocating cycles parallel to LIPSS with an Alumina ball; **b** the LIPSS profile along the white line in **(a)** Note: the measurement was taken in the middle of the wear track



point the surface hardness was already lower than that of the alumina ball.

The four samples were not investigated further, because only the friction behaviour rather than long-term wear performance was of interest in this study. It is worth mentioning that maximum Hertzian contact pressure calculated as alumina ball with flat DLC as a counterpart was around 620 MPa in this tests [32]. It is six to three times more than the contact/holding pressure in injection moulding processes [33]. Additionally, it can be stated that the measured CoF increase of 0.05 over the fs laser-processed DLC should not make this surface treatment as not appropriate for producing replication masters, but some additional micro-tribology tests with tips smaller than nanostructures should be performed to validate this further.

4 Conclusions

The effects of fs laser processing of DLC, especially on its properties, were investigated in this research as a potential treatment for replication masters. It was demonstrated that highly uniform LIPSS can be generated on thin DLC films without any delamination when optimised process settings are used, i.e. pulse numbers and fluence. The effects of this fs laser treatment were studied on representative DLC-coated samples and the following conclusions were made:

- Raman spectroscopy indicated that fs laser processing led to the formation of a thin graphitised surface layer that had changed properties to as-received DLC and

could explain the reduced hardness of fs laser-treated DLC samples.

- GAXRD showed that there were no appreciable changes in the DLC long-range ordering as a result of the fs laser processing, confirming that the change in crystallisation status, if any, should only occur within the thin laser-modified layer.
- The hardness of fs laser-treated DLC samples was dependent on the used laser processing settings, i.e. it decreased with the increase of pulse number and fluence, and overall it was significantly reduced after the fs laser treatment.
- Fs laser processing of DLC had only a marginal effect on CoF. However, even a small number of reciprocating cycles with an alumina ball led to flattening of sub-micron ripples on the fs laser-treated DLC samples.

Based on the findings of this research, the fs laser treatment of DLC coatings can be considered suitable and also advantageous for producing replication masters because of its lubricating properties and hardness that is still three times higher than the substrate material, i.e. stainless steel. Most of the DLC attractive properties can be retained, especially the relatively low CoF values and hence the low adhesive nature of DLC coatings even after their fs laser treatment. Thus, it can be stated that fs laser structuring/texturing of DLC coatings applied on replication masters is beneficial, as treated surfaces can be functionalised with sub-micron structures, i.e. LIPSS, while their improved wear resistance and demoulding performance are preserved. This enables manufacturing of masters that benefit both from the advantageous properties of the coatings and also from the added functionality of sub-micron structures/textures.

Acknowledgements The work was carried out within the H2020 FoF programme “High-Impact Injection Moulding Platform for mass-production of 3D and/or large micro-structured surfaces with Antimicrobial, Self-cleaning, Anti-scratch, Anti-squeak and Aesthetic functionalities” (HIMALAIA), the ITN programme “European ESRs Network on Short Pulsed Laser Micro/Nanostructuring of Surfaces for Improved Functional Applications” (Laser4Fun) and the UKIERI DST programme “Surface functionalisation for food, packaging, and healthcare applications”. Also, the authors would like to thank the Manufacturing Technology Centre (MTC) for the financial support of Aleksandra Michalek’s PhD research.

Open Access This article is licensed under a Creative Commons Attribution 4.0 International License, which permits use, sharing, adaptation, distribution and reproduction in any medium or format, as long as you give appropriate credit to the original author(s) and the source, provide a link to the Creative Commons licence, and indicate if changes were made. The images or other third party material in this article are included in the article’s Creative Commons licence, unless indicated otherwise in a credit line to the material. If material is not included in the article’s Creative Commons licence and your intended use is not permitted by statutory regulation or exceeds the permitted use, you will

need to obtain permission directly from the copyright holder. To view a copy of this licence, visit <http://creativecommons.org/licenses/by/4.0/>.

References

1. A.C. Ferrari, J. Robertson, Interpretation of Raman spectra of disordered and amorphous carbon. *Phys. Rev. B*. **61**, 95–107 (2000)
2. S.F. Ahmed, M.W. Moon, K.R. Lee, Effect of silver doping on optical property of diamond like carbon films. *Thin Solid Films* **517**, 4035–4038 (2009). <https://doi.org/10.1016/j.tsf.2009.01.135>
3. J. Robertson, Diamond-like amorphous carbon. *Mater. Sci. Eng. R Rep.* **37**, 129–281 (2002). [https://doi.org/10.1016/S0927-796X\(02\)00005-0](https://doi.org/10.1016/S0927-796X(02)00005-0)
4. K. Czyz, J. Marczak, R. Major, A. Mzyk, A. Rycyk, A. Sarzyński, M. Strzelec, Selected laser methods for surface structuring of bio-compatible diamond-like carbon layers. *Diam. Relat. Mater.* **67**, 26–40 (2016). <https://doi.org/10.1016/j.diamond.2016.01.013>
5. R.B. Jackman, L.H. Chua, Diamond-like carbon within micro-electronics: Dielectric properties on silicon and GaAs. *Diam. Relat. Mater.* **1**, 895–899 (1992). [https://doi.org/10.1016/0925-9635\(92\)90131-7](https://doi.org/10.1016/0925-9635(92)90131-7)
6. A.C. Ferrari, Diamond-like carbon for magnetic storage disks. *Surf. Coat. Technol.* **180–181**, 190–206 (2004). <https://doi.org/10.1016/j.surfcoat.2003.10.146>
7. B. Saha, E. Liu, S.B. Tor, N.W. Khun, D.E. Hardt, J.H. Chun, Anti-sticking behavior of DLC-coated silicon micro-molds. *J. Micromechanics Microengineering*. (2009). <https://doi.org/10.1088/0960-1317/19/10/105025>
8. C.A. Griffiths, A. Rees, R.M. Kerton, O.V. Fonseca, Temperature effects on DLC coated micro moulds. *Surf. Coat. Technol.* **307**, 28–37 (2016). <https://doi.org/10.1016/j.surfcoat.2016.08.034>
9. C.A. Griffiths, S.S. Dimov, E.B. Brousseau, C. Chouquet, J. Gavillet, S. Bigot, Investigation of surface treatment effects in micro-injection-moulding. *Int. J. Adv. Manuf. Technol.* **47**, 99–110 (2010). <https://doi.org/10.1007/s00170-009-2000-4>
10. C.A. Griffiths, S.S. Dimov, A. Rees, O. Dellea, J. Gavillet, F. Lacan, H. Hirshy, A novel texturing of micro injection moulding tools by applying an amorphous hydrogenated carbon coating. *Surf. Coat. Technol.* **235**, 1–9 (2013). <https://doi.org/10.1016/j.surfcoat.2013.07.006>
11. T. Roch, V. Weihnacht, H.J. Scheibe, A. Roch, A.F. Lasagni, Direct laser interference patterning of tetrahedral amorphous carbon films for tribological applications. *Diam. Relat. Mater.* **33**, 20–26 (2013). <https://doi.org/10.1016/j.diamond.2012.12.002>
12. N. Yasumaru, K. Miyazaki, J. Kiuchi, K. Komai, Tribological properties of diamond-like carbon films with surface nano-structure formed by femtosecond laser pulses. *J. Laser Micro Nanoeng.* **2**, 162–165 (2007). <https://doi.org/10.2961/jlmm.2007.02.0011>
13. N. Yasumaru, K. Miyazaki, J. Kiuchi, E. Sentoku, Frictional properties of diamond-like carbon, glassy carbon and nitrides with femtosecond-laser-induced nanostructure. *Diam. Relat. Mater.* **20**, 542–545 (2011). <https://doi.org/10.1016/j.diamond.2011.02.010>
14. N. Yasumaru, K. Miyazaki, J. Kiuchi, Control of tribological properties of diamond-like carbon films with femtosecond-laser-induced nanostructuring. *Appl. Surf. Sci.* **254**, 2364–2368 (2008). <https://doi.org/10.1016/j.apsusc.2007.09.037>
15. B. Dusser, Z. Sagan, H. Soder, N. Faure, J.P. Colombier, M. Jourlin, E. Audouard, Controlled nanostructures formation by ultra fast laser pulses for color marking. *Opt. Express*. **18**, 2913 (2010). <https://doi.org/10.1364/OE.18.002913>
16. A. Batal, R. Sammons, S. Dimov, Response of Saos-2 osteoblast-like cells to laser surface texturing, sandblasting and

- hydroxyapatite coating on CoCrMo alloy surfaces. *Mater. Sci. Eng. C*. **98**, 1005–1013 (2019). <https://doi.org/10.1016/j.msec.2019.01.067>
17. A.M. Prokhorov, A.S. Svakhin, V.A. Sychugov, A.V. Tishchenko, A.A. Khakimov, Excitation and resonant transformation of a surface electromagnetic wave during irradiation of a solid by high-power laser radiation. *Sov. J. Quantum Electron.* **13**, 568–571 (1983). <https://doi.org/10.1070/QE1983v013n05ABEH004226>
 18. S. Gräf, F.A. Müller, Polarisation-dependent generation of fs-laser induced periodic surface structures. *Appl. Surf. Sci.* **331**, 150–155 (2015). <https://doi.org/10.1016/j.apsusc.2015.01.056>
 19. T.V. Kononenko, V.V. Kononenko, S.M. Pimenov, E.V. Zavedeev, V.I. Konov, V. Romano, G. Dumitru, Effects of pulse duration in laser processing of diamond-like carbon films. *Diam. Relat. Mater.* **14**, 1368–1376 (2005). <https://doi.org/10.1016/j.diamond.2005.02.009>
 20. A. Dekanski, J. Stevanovic, R. Stevanovic, B.Z. Nikolic, V.M. Jovanovic, Glassy carbon electrodes I Characterization and electrochemical activation. *Carbon N. Y.* **39**, 1195–1205 (2001). [https://doi.org/10.1016/0008-6223\(94\)90011-6](https://doi.org/10.1016/0008-6223(94)90011-6)
 21. K.M. Tanvir Ahmmed, C. Grambow, A.M. Kietzig, Fabrication of micro/nano structures on metals by femtosecond laser micromachining. *Micromachines* **5** (2014) 1219–1253. doi:10.3390/mi5041219.
 22. P. Gregorčič, M. Sedlaček, B. Podgornik, J. Reif, Formation of laser-induced periodic surface structures (LIPSS) on tool steel by multiple picosecond laser pulses of different polarizations. *Appl. Surf. Sci.* **387**, 698–706 (2016). <https://doi.org/10.1016/j.apsusc.2016.06.174>
 23. M.S. Komlenok, N.R. Arutyunyan, V.V. Kononenko, E.V. Zavedeev, V.D. Frolov, A.A. Chouprik, A.S. Baturin, H.J. Scheibe, S.M. Pimenov, Structure and friction properties of laser-patterned amorphous carbon films. *Diam. Relat. Mater.* **65**, 69–74 (2016). <https://doi.org/10.1016/j.diamond.2016.02.006>
 24. L.C. Nistor, J. Van Landuyt, V.G. Ralchenko, T.V. Kononenko, E.D. Obratsova, V.E. Strelnitsky, Direct observation of laser-induced crystallization of a-C: H films. *Appl. Phys. A Solids Surf.* **58**, 137–144 (1994). <https://doi.org/10.1007/BF00332170>
 25. H.O. Jeschke, M.E. Garcia, K.H. Bennemann, Theory for laser-induced ultrafast phase transitions in carbon. *Appl. Phys. A Mater. Sci. Process.* (1999). <https://doi.org/10.1007/s003399900340>
 26. C.Z. Wang, K.M. Ho, M.D. Shirk, P.A. Molian, Laser-induced graphitization on a diamond (111) surface. *Phys. Rev. Lett.* **85**, 4092–4095 (2000). <https://doi.org/10.1103/PhysRevLett.85.4092>
 27. G. Dumitru, V. Romano, H.P. Weber, S. Pimenov, T. Kononenko, M. Sentis, J. Örg Hermann, S. Bruneau, Femtosecond laser ablation of diamond-like carbon films. *Appl. Surf. Sci.* **222** (2004) 226–233. doi:10.1016/j.apsusc.2003.08.031.
 28. N. Yasumaru, K. Miyazaki, J. Kiuchi, Glassy carbon layer formed in diamond-like carbon films with femtosecond laser pulses. *Appl. Phys. A Mater. Sci. Process.* **79**, 425–427 (2004). <https://doi.org/10.1007/s00339-004-2746-3>
 29. J. Csontos, Z. Pápa, A. Gárdián, M. Füle, J. Budai, Z. Toth, Spectroscopic ellipsometric and Raman spectroscopic investigations of pulsed laser treated glassy carbon surfaces. *Appl. Surf. Sci.* **336**, 343–348 (2015). <https://doi.org/10.1016/j.apsusc.2014.12.133>
 30. H. Pang, X. Wang, G. Zhang, H. Chen, G. Lv, S. Yang, Characterization of diamond-like carbon films by SEM, XRD and Raman spectroscopy. *Appl. Surf. Sci.* **256**, 6403–6407 (2010). <https://doi.org/10.1016/j.apsusc.2010.04.025>
 31. M. Hokao, S. Hironaka, Y. Suda, Y. Yamamoto, Friction and wear properties of graphite/glassy carbon composites. *Wear* **237**, 54–62 (2000). [https://doi.org/10.1016/S0043-1648\(99\)00306-3](https://doi.org/10.1016/S0043-1648(99)00306-3)
 32. R.G. Budynas, K. Nisbeth, *Shigley's Mechanical Engineering Design*, 9th edn. (McGraw-Hill, NY, 2011)
 33. V. Bellantone, R. Surace, G. Trotta, I. Fassi, Replication capability of micro injection moulding process for polymeric parts manufacturing. *Int. J. Adv. Manuf. Technol.* **67**, 1407–1421 (2013). <https://doi.org/10.1007/s00170-012-4577-2>

Publisher's Note Springer Nature remains neutral with regard to jurisdictional claims in published maps and institutional affiliations.